

# IOWA STATE UNIVERSITY

## Digital Repository

---

Electrical and Computer Engineering Publications

Electrical and Computer Engineering

---

1-2007

## Bayesian NDE Defect Signal Analysis

Aleksandar Dogandžić  
*Iowa State University*, [ald@iastate.edu](mailto:ald@iastate.edu)

Benhong Zhang  
*Iowa State University*

Follow this and additional works at: [http://lib.dr.iastate.edu/ece\\_pubs](http://lib.dr.iastate.edu/ece_pubs)



Part of the [Signal Processing Commons](#), and the [Systems and Communications Commons](#)

The complete bibliographic information for this item can be found at [http://lib.dr.iastate.edu/ece\\_pubs/135](http://lib.dr.iastate.edu/ece_pubs/135). For information on how to cite this item, please visit <http://lib.dr.iastate.edu/howtocite.html>.

---

This Article is brought to you for free and open access by the Electrical and Computer Engineering at Iowa State University Digital Repository. It has been accepted for inclusion in Electrical and Computer Engineering Publications by an authorized administrator of Iowa State University Digital Repository. For more information, please contact [digirep@iastate.edu](mailto:digirep@iastate.edu).

# Bayesian NDE Defect Signal Analysis<sup>†</sup>

*Aleksandar Dogandžić and Benhong Zhang*

ECpE Department, Iowa State University

3119 Coover Hall, Ames, IA 50011

Phone: (515) 294-0500 Fax: (515) 294-8432

email: {ald, zhangbh}@iastate.edu

## Abstract

We develop a hierarchical Bayesian approach for estimating defect signals from noisy measurements and apply it to nondestructive evaluation (NDE) of materials. We propose a parametric model for the shape of the defect region and assume that the defect signals within this region are random with unknown mean and variance. Markov chain Monte Carlo (MCMC) algorithms are derived for simulating from the posterior distributions of the model parameters and defect signals. These algorithms are then utilized to identify potential defect regions and estimate their size and reflectivity parameters. Our approach provides Bayesian confidence regions (credible sets) for the estimated parameters, which are important in NDE applications. We specialize the proposed framework to elliptical defect shape and Gaussian signal and noise models and apply it to experimental ultrasonic *C*-scan data from an inspection of a cylindrical titanium billet. We also outline a simple classification scheme for separating defects from non-defects using estimated mean signals and areas of the potential defects.

## I. INTRODUCTION

In nondestructive evaluation (NDE) applications, defect signal typically affects multiple measurements at neighboring spatial locations. Therefore, multiple spatial measurements should be incorporated into defect detection and estimation (sizing) algorithms. In [1], measurements within a sliding window were compared with a dynamically chosen threshold in order to detect potential defects in ultrasonic *C* scans. Related problems have been studied in image processing literature in the context of image segmentation and saliency region detection, see e.g. [2]–[3] and [4] (respectively) and references therein. In this correspondence (see also [5]), we propose

- a *parametric model* that describes defect shape, location, and reflectivity,
- a *hierarchical Bayesian* framework and Markov chain Monte Carlo (MCMC) algorithms for estimating these parameters assuming a single defect,
- a sequential method for identifying multiple potential defect regions and estimating their parameters, and
- a simple classification scheme for separating defects from non-defects using estimated mean signals and areas of the potential defects.

We adopt elliptical defect shape and Gaussian signal and noise models; however, the proposed framework is applicable to other scenarios as well. The elliptical shape model is well-suited for describing hard alpha inclusions in titanium alloys [6]. In most applications, the defect signal is not uniform over the defect region but varies *randomly* depending,

<sup>†</sup>This work was supported by the NSF Industry-University Cooperative Research Program, Center for Nondestructive Evaluation (CNDE), Iowa State University.

for example, on local reflectivity and various constructive and destructive interferences. To account for these variations, we assume that the defect signal is *random* over the defect region, having fixed (but unknown) mean and variance.

In Section II, we describe the measurement model and prior specifications. In Section III and Appendix A, we develop Bayesian methods for simulating and estimating the defect model parameters and signals (Sections III-A–III-C). In addition, our approach provides *Bayesian confidence regions (credible sets)* for the estimated parameters, which are important in NDE applications. The underlying Bayesian paradigm allows us to easily incorporate available prior information about the defect reflectivity, shape, or size. In Section IV, the proposed methods are applied to experimental ultrasonic *C*-scan data from an inspection of a cylindrical titanium billet. Although we focus on estimating parameters of a single defect, we also discuss the multiple-defect scenario in Section IV. Note that applying optimal Bayesian approaches for estimating the number and parameters of multiple defects (e.g. reversible-jump MCMC schemes [9, Ch. 11]) would lead to computationally intractable solutions. In Section IV, we propose a simple sequential method and a classification scheme for identifying multiple potential defect regions and separating defects from non-defects. Concluding remarks are given in Section V.

## II. MEASUREMENT MODEL AND PRIOR SPECIFICATIONS

We first introduce our parametric defect location and shape models (Section II-A) and random noise and defect-signal models (Sections II-B and II-C). Then, in Section II-D, we combine the noise and signal models by integrating out the random signals. Our goal is to estimate the model (defect location, shape, and signal-distribution) parameters and random signals. In Section II-E, we introduce our model-parameter prior specifications.

The random defect signals and model parameters that we wish to estimate are described using a *hierarchical statistical model*, see [7, Ch. 5] for an introduction to hierarchical models.

### A. Parametric Model for Defect Location and Shape

Assume that a potential defect-signal region  $\mathcal{R}(\mathbf{z})$  can be modeled as an ellipse:

$$\mathcal{R}(\mathbf{z}) = \{\mathbf{r} : (\mathbf{r} - \mathbf{r}_0)^T \Sigma_{\mathbf{R}}(d, A, \varphi)^{-1} (\mathbf{r} - \mathbf{r}_0) \leq 1\} \quad (2.1)$$

where  $\mathbf{r} = [x_1, x_2]^T$  denotes location in Cartesian coordinates,

$$\mathbf{z} = [\mathbf{r}_0^T, d, A, \varphi]^T \quad (2.2)$$

is the vector of (unknown) defect location and shape parameters,<sup>1</sup>

$$\Sigma_{\mathbf{R}}(d, A, \varphi) = \Phi(\varphi) \cdot \begin{bmatrix} d^2 & 0 \\ 0 & A^2/(d^2\pi^2) \end{bmatrix} \cdot \Phi(\varphi)^T, \quad \Phi(\varphi) = \begin{bmatrix} \cos \varphi & -\sin \varphi \\ \sin \varphi & \cos \varphi \end{bmatrix} \quad (2.3)$$

and “ $T$ ” denotes a transpose. Here,  $\mathbf{r}_0 = [x_{0,1}, x_{0,2}]^T$  represents the center of the ellipse in Cartesian coordinates,  $d > 0$  is an axis parameter,  $A > 0$  the area of the ellipse, and  $\varphi \in [-\pi/4, \pi/4]$  the ellipse orientation parameter (in radians). Under the above parametrization,  $d$  and  $A/(d\pi)$  are the axes of the ellipse  $\mathcal{R}(\mathbf{z})$ .

<sup>1</sup>The inverse of  $\Sigma_{\mathbf{R}}$  can be easily computed as  $\Sigma_{\mathbf{R}}(d, A, \varphi)^{-1} = \Phi(\varphi) \cdot \begin{bmatrix} 1/d^2 & 0 \\ 0 & d^2\pi^2/A^2 \end{bmatrix} \cdot \Phi(\varphi)^T$ .

### B. Measurement-Error (Noise) Model

Assume that we have collected measurements  $y_i$  at locations  $\mathbf{s}_i$ ,  $i = 1, 2, \dots, \mathbb{N}_{\text{tot}}$  within the region of interest, where  $\mathbb{N}_{\text{tot}}$  denotes the total number of measurements in this region. We adopt the following measurement-error model:

- If  $y_i$  is collected over the defect region [i.e.  $\mathbf{s}_i \in \mathcal{R}(\mathbf{z})$ ], then

$$y_i = \theta_i + e_i \quad (2.4a)$$

where  $\theta_i$  and  $e_i$  denote the defect signal (related to its reflectivity) and noise at location  $\mathbf{s}_i$ , respectively;

- if  $y_i$  is collected outside the defect region [i.e.  $\mathbf{s}_i \in \mathcal{R}^c(\mathbf{z})$ , where  $\mathcal{R}^c(\mathbf{z})$  denotes the *noise-only region* outside  $\mathcal{R}(\mathbf{z})$ ], then the measurements contain only noise:

$$y_i = e_i \quad (2.4b)$$

implying that the signals  $\theta_i$  are zero in the noise-only region.

We model the additive noise samples  $e_i$ ,  $i = 1, 2, \dots, \mathbb{N}_{\text{tot}}$  as zero-mean independent, identically distributed (i.i.d.) Gaussian random variables with known variance  $\sigma^2$  (which can be easily estimated from the noise-only data). Denote by  $\mathcal{N}(y; \mu, \sigma^2)$  the Gaussian probability density function (pdf) of a random variable  $y$  with mean  $\mu$  and variance  $\sigma^2$ . Then, (2.4a) and (2.4b) imply that the conditional distribution of the measurement  $y_i$  given  $\theta_i$  is  $p(y_i | \theta_i) = \mathcal{N}(y_i; \theta_i, \sigma^2)$ , where  $\theta_i = 0$  for  $\mathbf{s}_i \in \mathcal{R}^c(\mathbf{z})$ . In the following, we describe a model for the signals  $\theta_i$ .

### C. Defect-Signal (Reflectivity) Model

Assume that the signals  $\theta_i$  within the defect region [for  $\mathbf{s}_i \in \mathcal{R}(\mathbf{z})$ ] are i.i.d. Gaussian with unknown mean  $\mu$  and variance  $\tau^2$ , which define the vector of unknown *defect-signal distribution parameters*:

$$\mathbf{w} = [\mu, \tau]^T. \quad (2.5)$$

Therefore, the joint pdf of the defect signals conditional on  $\mathbf{w}$  and  $\mathbf{z}$  can be written as

$$p(\{\theta_i, \mathbf{s}_i \in \mathcal{R}(\mathbf{z})\} | \mathbf{w}, \mathbf{z}) = \prod_{i, \mathbf{s}_i \in \mathcal{R}(\mathbf{z})} \mathcal{N}(\theta_i; \mu, \tau^2). \quad (2.6)$$

In the noise-only region [i.e.  $\mathbf{s}_i \in \mathcal{R}^c(\mathbf{z})$ ] the signals  $\theta_i$  are zero, see also the previous section.

In the hierarchical modeling context, the elements of  $\mathbf{w}$  are often referred to as *hyperparameters*. Note that  $\tau$  is a measure of defect-signal variability: if  $\tau = 0$ , then all  $\theta_i$  within the defect region are *equal to*  $\mu$ .

### D. Measurement Model for the Location, Shape, and Defect-Signal Distribution Parameters

Define the vector of all model parameters [see (2.2) and (2.5)]:

$$\boldsymbol{\phi} = [\mathbf{z}^T, \mathbf{w}^T]^T. \quad (2.7)$$

We now combine the noise and defect-signal models in Sections II-B and II-C and *integrate out* the  $\theta_i$ s. Consequently, conditional on the model parameters  $\phi$ , the observations  $y_i$  collected over the defect region are i.i.d. Gaussian random variables with the following pdf:

$$p(y_i | \phi) = \mathcal{N}(y_i; \mu, \sigma^2 + \tau^2), \quad \text{for } \mathbf{s}_i \in \mathcal{R}(\mathbf{z}) \quad (2.8a)$$

whereas the observations collected in the noise-only region are zero-mean i.i.d. Gaussian with pdf:

$$p(y_i | \phi) = \mathcal{N}(y_i; 0, \sigma^2), \quad \text{for } \mathbf{s}_i \in \mathcal{R}^c(\mathbf{z}). \quad (2.8b)$$

Since we can *integrate out* the random signals  $\theta_i, \mathbf{s}_i \in \mathcal{R}(\mathbf{z})$ , we can *decouple* sampling the model parameters  $\phi$  from sampling the  $\theta_i$ s, as demonstrated in Sections III-A and III-B.

#### E. Prior Specifications for the Model Parameters

We assume that the defect location, shape, and signal-distribution parameters are independent *a priori*:<sup>2</sup>

$$\pi_{\phi}(\phi) = \pi_{\mathbf{z}}(\mathbf{z}) \cdot \pi_{\mathbf{w}}(\mathbf{w}) \quad (2.9a)$$

where

$$\pi_{\mathbf{z}}(\mathbf{z}) = \pi_{x_{0,1}}(x_{0,1}) \cdot \pi_{x_{0,2}}(x_{0,2}) \cdot \pi_d(d) \cdot \pi_A(A) \cdot \pi_{\varphi}(\varphi), \quad \pi_{\mathbf{w}}(\mathbf{w}) = \pi_{\mu}(\mu) \cdot \pi_{\tau}(\tau). \quad (2.9b)$$

Let us adopt simple uniform-distribution priors for all the model parameters:

$$\pi_{\mu}(\mu) = \text{uniform}(0, \mu_{\text{MAX}}) \quad (2.10a)$$

$$\pi_{\tau}(\tau) = \text{uniform}(0, \tau_{\text{MAX}}) \quad (2.10b)$$

$$\pi_{x_{0,1}}(x_{0,1}) = \text{uniform}(x_{0,1,\text{MIN}}, x_{0,1,\text{MAX}}) \quad (2.10c)$$

$$\pi_{x_{0,2}}(x_{0,2}) = \text{uniform}(x_{0,2,\text{MIN}}, x_{0,2,\text{MAX}}) \quad (2.10d)$$

$$\pi_d(d) = \text{uniform}(d_{\text{MIN}}, d_{\text{MAX}}) \quad (2.10e)$$

$$\pi_A(A) = \text{uniform}(A_{\text{MIN}}, A_{\text{MAX}}) \quad (2.10f)$$

$$\pi_{\varphi}(\varphi) = \text{uniform}(\varphi_{\text{MIN}}, \varphi_{\text{MAX}}) \quad (2.10g)$$

where  $\varphi_{\text{MIN}} \geq -\pi/4$ ,  $\varphi_{\text{MAX}} \leq \pi/4$ ,  $d_{\text{MIN}} > 0$ , and  $A_{\text{MIN}} > 0$ .

### III. BAYESIAN ANALYSIS

The goals of our analysis in this section are to estimate the model parameters  $\phi$  and random signals  $\theta_i$ ,  $i = 1, 2, \dots, \mathbb{N}_{\text{tot}}$  describing a single defect region under the measurement model and prior specifications in Section II. The posterior pdf of  $\phi$  follows by using (2.8a)–(2.8b) and (2.9a):

$$\begin{aligned} p(\phi | \mathbf{y}) &\propto \pi_{\mathbf{z}}(\mathbf{z}) \cdot \pi_{\mathbf{w}}(\mathbf{w}) \cdot p(\mathbf{y} | \phi) = \pi_{\mathbf{z}}(\mathbf{z}) \cdot \pi_{\mathbf{w}}(\mathbf{w}) \cdot \prod_{i, \mathbf{s}_i \in \mathcal{R}(\mathbf{z})} \mathcal{N}(y_i; \mu, \sigma^2 + \tau^2) \cdot \prod_{i, \mathbf{s}_i \in \mathcal{R}^c(\mathbf{z})} \mathcal{N}(y_i; 0, \sigma^2) \\ &\propto \pi_{\mathbf{z}}(\mathbf{z}) \cdot \pi_{\mathbf{w}}(\mathbf{w}) \cdot l(\mathbf{y} | \mathbf{z}, \mathbf{w}) \end{aligned} \quad (3.1a)$$

<sup>2</sup>Here,  $\pi_{\phi}(\phi)$  denotes the prior pdf of  $\phi$  and analogous notation is used for the prior pdfs of the components of  $\phi$ .

which simply states that the posterior pdf of  $\phi$  is proportional to the product of the prior and likelihood of  $\phi$ . Here,  $\mathbf{y} = [y_1, y_2, \dots, y_{N_{\text{tot}}}]^T$  denotes the vector of all observations,

$$l(\mathbf{y} | \mathbf{z}, \mathbf{w}) = \prod_{i, \mathbf{s}_i \in \mathcal{R}(\mathbf{z})} \frac{\mathcal{N}(y_i; \mu, \sigma^2 + \tau^2)}{\mathcal{N}(y_i; 0, \sigma^2)} = \left(1 + \frac{\tau^2}{\sigma^2}\right)^{-N(\mathbf{z})/2} \cdot \exp \left\{ -\frac{1}{2} \sum_{i, \mathbf{s}_i \in \mathcal{R}(\mathbf{z})} \left[ \frac{(y_i - \mu)^2}{\sigma^2 + \tau^2} - \frac{y_i^2}{\sigma^2} \right] \right\} \quad (3.1b)$$

is the normalized likelihood (i.e. likelihood ratio), and

$$N(\mathbf{z}) = \sum_{i, \mathbf{s}_i \in \mathcal{R}(\mathbf{z})} 1 \quad (3.2)$$

is the number of measurements collected over the defect region  $\mathcal{R}(\mathbf{z})$ .

In Sections III-A and III-B (below), we construct methods for drawing samples from the posterior distributions of the model parameters  $\phi$  and random signals

$$\boldsymbol{\theta} = [\theta_1, \theta_2, \dots, \theta_{N_{\text{tot}}}]^T. \quad (3.3)$$

We utilize these samples to estimate  $\phi$  and  $\boldsymbol{\theta}$  (Section III-C) and construct credible sets for these parameters.

#### A. Simulating the Model Parameters $\phi$

We first outline our proposed scheme for simulating from the joint posterior pdf  $p(\phi | \mathbf{y})$ . To draw samples from this distribution, we apply a Gibbs sampler [7]–[9] which utilizes the full conditional posterior pdfs of  $\tau, \mu$  and  $\mathbf{z}$ :

$$1) \quad \text{Draw } \tau^{(t)} \text{ from} \quad p(\tau | \mu^{(t-1)}, \mathbf{z}^{(t-1)}, \mathbf{y}) \quad (3.4a)$$

using *rejection sampling* [10], [7, Ch. 11.1] (as described in Appendix A-A), where  $\mu^{(t-1)}$  and  $\mathbf{z}^{(t-1)}$  have been obtained in Steps 2) and 3) of the  $(t-1)$ th cycle.

$$2) \quad \text{Draw } \mu^{(t)} \text{ from} \quad p(\mu | \tau^{(t)}, \mathbf{z}^{(t-1)}, \mathbf{y}) \quad (3.4b)$$

which is a *truncated Gaussian distribution*, easy to sample from using e.g. the algorithm in [11] (see also Appendix A-B).

$$3) \quad \text{Draw } \mathbf{z}^{(t)} \text{ from} \quad p(\mathbf{z} | \mathbf{w}^{(t)}, \mathbf{y}) \quad \text{where} \quad \mathbf{w}^{(t)} = [\mu^{(t)}, \tau^{(t)}]^T \quad (3.4c)$$

using *shrinkage slice sampling* [12], see Appendix A-C.

Cycling through the Steps 1)–3) is performed until the desired number of samples  $\phi^{(t)} = [(\mathbf{z}^{(t)})^T, (\mathbf{w}^{(t)})^T]^T$  is collected (after discarding the samples from the burn-in period, see e.g. [7]–[9]). This scheme produces a *Markov chain*  $\phi^{(0)}, \phi^{(1)}, \phi^{(2)}, \dots$  with stationary distribution equal to  $p(\phi | \mathbf{y})$ .

### B. Simulating the Random Signals $\theta_i$

To estimate the random signals  $\theta$ , we utilize *composition sampling* from the posterior pdf  $p(\theta | \mathbf{y}) = \int p(\theta | \phi, \mathbf{y}) p(\phi | \mathbf{y}) d\phi$ , which can be done as follows (see also [7, steps 1. and 2. on p. 127]):

- Draw  $\phi^{(t)}$  from  $p(\phi | \mathbf{y})$ , as described in Section III-A;
- Draw  $\theta^{(t)}$  from  $p(\theta | \phi^{(t)}, \mathbf{y})$  as follows:
  - for  $i \in \mathcal{R}(\mathbf{z}^{(t)})$ , draw conditionally independent samples  $\theta_i^{(t)}$  from

$$p(\theta_i^{(t)} | \phi^{(t)}, y_i) = \mathcal{N}\left(\theta_i^{(t)}; \frac{(\tau^{(t)})^2 y_i + \sigma^2 \mu^{(t)}}{(\tau^{(t)})^2 + \sigma^2}, \left[\frac{1}{(\tau^{(t)})^2} + \frac{1}{\sigma^2}\right]^{-1}\right) \quad (3.5a)$$

- for  $i \in \mathcal{R}^c(\mathbf{z}^{(t)})$ , set  $\theta_i^{(t)} = 0$

yielding  $\theta^{(t)} = [\theta_1^{(t)}, \theta_2^{(t)}, \dots, \theta_{N_{\text{tot}}}^{(t)}]^T$ .

Then, the mean signal  $\bar{\theta} = [1/N(\mathbf{z})] \cdot \sum_{i, \mathbf{s}_i \in \mathcal{R}(\mathbf{z})} \theta_i$  within the potential defect region simulated in the  $t$ th draw can be estimated as  $\bar{\theta}^{(t)} = [1/N(\mathbf{z}^{(t)})] \cdot \sum_{i, \mathbf{s}_i \in \mathcal{R}(\mathbf{z}^{(t)})} \theta_i^{(t)}$ .

Note that the proposed MCMC algorithms are *automatic*, i.e. their implementation does not require preliminary runs and additional tuning. This is unlike the Metropolis-Hastings algorithm and algorithms that contain Metropolis steps, which typically require tuning the scales of the proposal distributions [13].

### C. Estimating the Model Parameters $\phi$ and Random Signals $\theta$

Once we have collected enough samples, we estimate the posterior means of  $\phi$  and  $\theta$  simply by averaging the last  $T$  draws:

$$\mathbb{E}[\phi | \mathbf{y}] \approx \hat{\phi} = [\hat{\mathbf{z}}^T, \hat{\mathbf{w}}^T]^T = \frac{1}{T} \sum_{t=t_0+1}^{t_0+T} \phi^{(t)}, \quad \mathbb{E}[\theta | \mathbf{y}] \approx \hat{\theta} = \frac{1}{T} \sum_{t=t_0+1}^{t_0+T} \theta^{(t)} \quad (3.6)$$

where  $t_0$  defines the burn-in period. Note that  $\hat{\phi}$  and  $\hat{\theta}$  are the (approximate) minimum mean-square error (MMSE) estimates of  $\phi$  and  $\theta$ .

## IV. NUMERICAL EXAMPLES

We apply the proposed approach to experimental ultrasonic  $C$ -scan data from an inspection of a cylindrical Ti 6-4 billet. The sample, developed as a part of the work of the Engine Titanium Consortium, contains 17 # 2 flat bottom holes at 3.2" depth. (The flat bottom holes are machined "defects" whose locations are exactly known.) The ultrasonic data were collected in a single experiment by moving a probe along the axial direction and scanning the billet along the circumferential direction at each axial position. The raw  $C$ -scan data with marked true defect regions are shown in Fig. 1. The vertical coordinate is proportional to rotation angle and the horizontal coordinate to axial position.

Before analyzing the data, we divided the  $C$ -scan image into three regions, as shown in Fig. 2. In each region, we subtracted row means from the measurements within the same row. We note that the noise level in Region 2 is

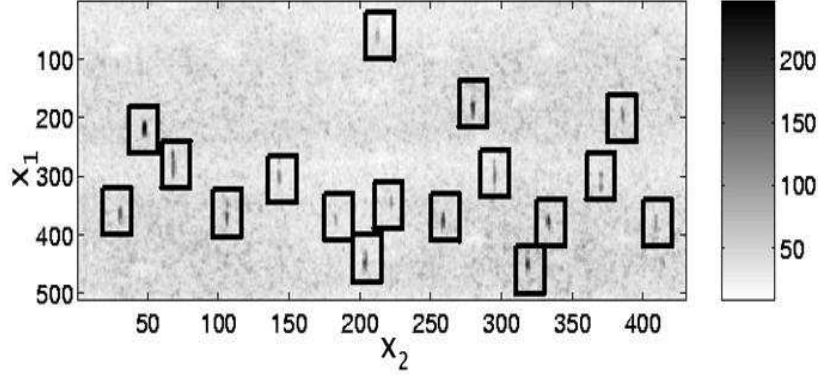


Fig. 1. Ultrasonic  $C$ -scan data with 17 defects.

lower than the corresponding noise levels in Regions 1 and 3. Indeed, the sample estimates of the noise variance  $\sigma^2$  in Regions 1, 2, and 3 are<sup>3</sup>:  $11.9^2$ ,  $10.3^2$ , and  $12.0^2$ , respectively. This phenomenon, known as *grain-noise banding* [1], is common in titanium billet inspections; it is a result of the billet manufacturing process. We now analyze each region separately assuming known noise variances  $\sigma^2$  (set to the above sample estimates). We chose the prior pdfs in (2.10) with  $\mu_{\text{MAX}} = \max\{y_1, y_2, \dots, y_{N_{\text{tot}}}\}$ ,  $\tau_{\text{MAX}} = 3\sigma$ ,  $d_{\text{MIN}} = 1$ ,  $d_{\text{MAX}} = 10$ ,  $A_{\text{MIN}} = 30$ ,  $A_{\text{MAX}} = 300$ ,  $\varphi_{\text{MIN}} = -\pi/8$ ,  $\varphi_{\text{MAX}} = \pi/8$ , and selected  $x_{0,i,\text{MIN}}$ ,  $x_{0,i,\text{MAX}}$ ,  $i = 1, 2$  to span the region that is being analyzed. The minimum and maximum areas of the defect region ( $A_{\text{MIN}}$  and  $A_{\text{MAX}}$ ) need to be specified carefully. If we set  $A_{\text{MAX}}$  to be too large, it may take a long time for our algorithms to converge. If we choose too small  $A_{\text{MIN}}$ , our chains may converge to some of the grains (in the grain structure of the material), requiring the use of a larger number of chains to ensure that the true defects are not missed.

We now describe our analysis of Region 1, where we ran seven Markov chains. We perform *sequential identification* of potential defects, as described in the following discussion. We first ran 10,000 cycles of the Gibbs sampler described in Section III-A and utilized the last  $T = 2,000$  samples to estimate the posterior distributions  $p(\phi | \mathbf{y})$  and  $p(\theta | \mathbf{y})$ ; hence, the burn-in period is  $t_0 = 8,000$  samples. The posterior means  $E[\theta_i | \mathbf{y}]$  of the random signals  $\theta_i$ , which are also the MMSE estimates of  $\theta_i$ , have been estimated by averaging the  $T$  draws [see (3.6)]:

$$\hat{\theta}_i|_{\text{chain } 1} \approx \frac{1}{T} \sum_{t=t_0+1}^{t_0+T} \theta_i^{(t)}, \quad i = 1, 2, \dots, N_{\text{tot}}. \quad (4.1)$$

Before running the second chain, we *subtracted* the first chain's MMSE estimates  $\hat{\theta}_i|_{\text{chain } 1}$  from the measurements  $y_i$ ,  $i = 1, 2, \dots, N_{\text{tot}}$ , effectively removing the first potential defect region from the data. We then ran the second Markov chain using the filtered data  $y_i|_{\text{chain } 2} = y_i - \hat{\theta}_i|_{\text{chain } 1}$ , computed the MMSE estimates  $\hat{\theta}_i|_{\text{chain } 2}$  of the second potential defect signal (using the second Markov chain), subtracted them out (yielding  $y_i|_{\text{chain } 3} = y_i|_{\text{chain } 2} - \hat{\theta}_i|_{\text{chain } 2}$ ), and continued this procedure until reaching the desired number of chains. In Fig. 3 (a), we

<sup>3</sup>These sample estimates are computed as follows:  $\sigma^2 = (1/N_{\text{tot}}) \cdot \sum_{i=1}^{N_{\text{tot}}} y_i^2$ . We note that the defects are much smaller in size than the three Regions in Fig. 2; consequently, the defect signals in these regions introduce negligible bias to the estimation of  $\sigma^2$ .



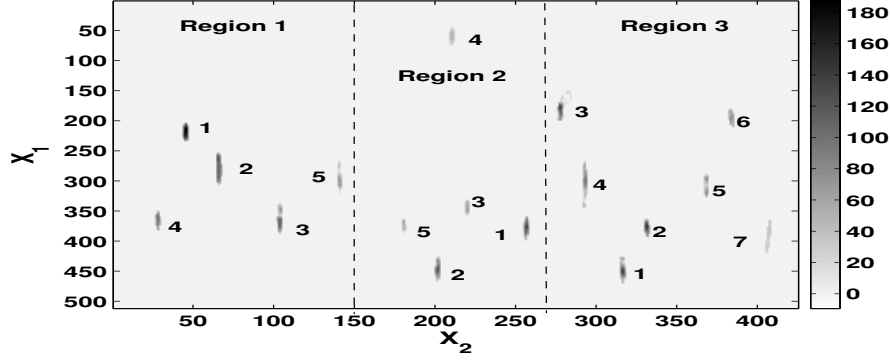


Fig. 2. MMSE estimates  $\hat{\theta}_i$  of the random signals  $\theta_i$  for the chains having the smallest model-parameter deviances.

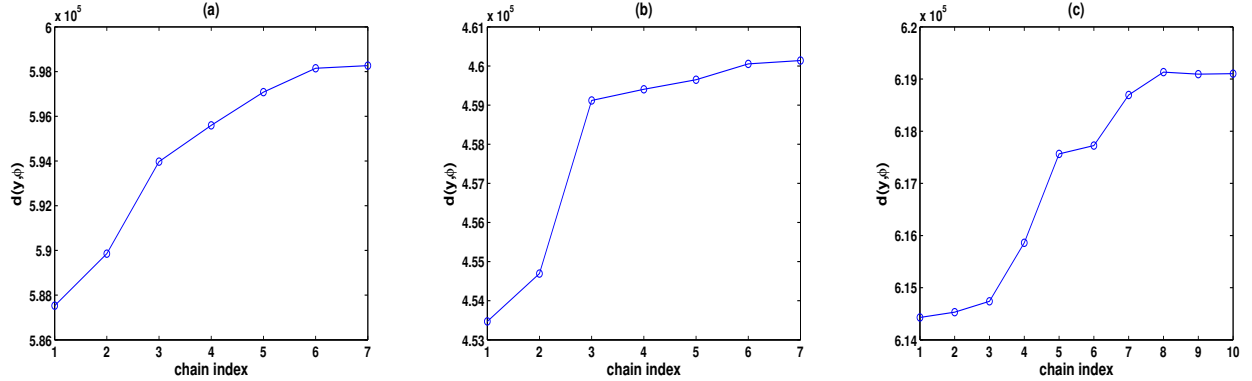


Fig. 3. Estimated model-parameter deviances for the potential defects in Region 1, 2, and 3, respectively.

show estimated model-parameter deviances (see e.g. [7, eq. (6.7)]):<sup>4</sup>

$$d(\mathbf{y}, \hat{\phi}) = -2 \ln p(\mathbf{y} | \hat{\phi}) = N_{\text{tot}} \cdot \ln(2\pi\sigma^2) + \sum_{i=1}^{N_{\text{tot}}} \frac{y_i^2}{\sigma^2} - 2 \ln l(\mathbf{y} | \hat{\mathbf{z}}, \hat{\mathbf{w}}) \quad (4.2)$$

for the seven chains in Region 1, where the estimates  $\hat{\phi}$  were computed for each chain using (3.6). The chains have been sorted in the increasing order according to the estimated model-parameter deviances. Note that the true defects have small estimated deviances; hence we may use these deviances to rank the potential defects according to their severity.

We have applied the proposed sequential scheme to Regions 2 and 3, where we ran seven and ten chains, respectively. The obtained estimated (and sorted) model-parameter deviances for these chains are shown in parts (b) and (c) of Fig. 3.

Fig. 2 shows the MMSE estimates of the defect signals for the first five potential defects (chains) from Region 1 (i.e.  $\hat{\theta}_i|_{\text{chain } 1}, \hat{\theta}_i|_{\text{chain } 2}, \dots, \hat{\theta}_i|_{\text{chain } 5}$ , see also (4.1)) and first five and seven potential defects from Regions 2 and 3, respectively. The ranks (chain indices) of the potential defects within each region are also shown in Fig. 2. Remarkably, the locations of these 17 potential defects correspond to the true locations of the flat bottom holes (i.e.

<sup>4</sup>See [7, Ch. 6.7], [8, Ch. 6.5.1], and [14] for definitions of deviance-based goodness-of-fit measures and examples of their use.

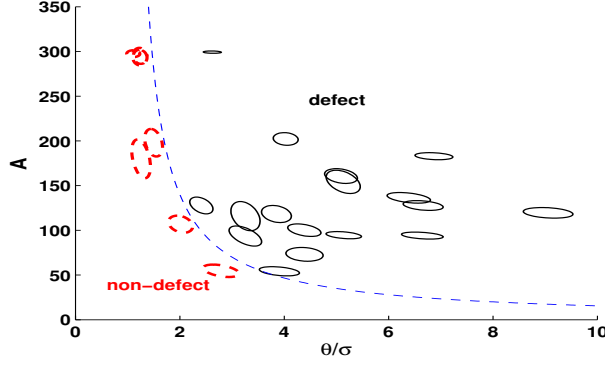


Fig. 4. Approximate 90% credible sets for the normalized mean signals  $\bar{\theta}/\sigma$  and areas  $A$  of all potential defects in the three regions and a possible classification boundary for separating defects from non-defects.

the true defects) in Fig. 1.

Even though the estimated model-parameter deviances in Fig. 3 allow us to assess the severity of potential defect regions, they do not provide sufficient information for deciding between defects and non-defects. To be able to separate defects from non-defects, we need to examine the mean signals and areas of the potential defect regions as well.<sup>5</sup> In Fig. 4, we plot approximate 90% Bayesian confidence regions (credible sets)<sup>6</sup> for the normalized mean signals  $\bar{\theta}/\sigma$  and areas  $A$

$$([A, \bar{\theta}/\sigma]^T - [\hat{A}, \hat{\bar{\theta}}/\sigma]^T)^T \cdot C^{-1} \cdot ([A, \bar{\theta}/\sigma]^T - [\hat{A}, \hat{\bar{\theta}}/\sigma]^T) \leq \xi \quad (4.3)$$

of all 24 potential defects in the three regions. Here,

- $\hat{A}$  and  $\hat{\bar{\theta}}$  denote the MMSE estimates of  $A$  and  $\bar{\theta}$  [computed using (3.6)];
- $C$  is the sample covariance matrix of the posterior samples  $[A^{(t)}, \bar{\theta}^{(t)}]^T$ :

$$C = \frac{1}{T} \cdot \sum_{t=t_0+1}^{t_0+T} ([A^{(t)}, \bar{\theta}^{(t)}]^T - [\hat{A}, \hat{\bar{\theta}}]^T) ([A^{(t)}, \bar{\theta}^{(t)}] - [\hat{A}, \hat{\bar{\theta}}]) \quad (4.4)$$

- $\xi$  is a constant chosen (for each chain) so that 90% of the samples  $[A^{(t)}, \bar{\theta}^{(t)}]^T$ ,  $t = t_0, \dots, T$  satisfy (4.3). (A good approximate choice of  $\xi$  is  $\xi \approx 4$ , which is based on the normal-distribution approximation.)

In Fig. 4, we also show that it is possible to separate defects from non-defect using a simple classification boundary,  $A \cdot (\bar{\theta}/\sigma) - A - 140 = 0$ . As the defect strength decreases, the required area (for a real defect) increases; similarly, as the area decreases, the required signal strength increases.

We now present our final example showing the performance of the proposed approach when signal-to-noise ratio is low. Here, we added i.i.d. zero-mean Gaussian noise with variance  $\sigma^2 = 250^2$  to the defect signals in Fig. 5 (a) (corresponding to one of the flat bottom holes from the previous examples), yielding the simulated noisy observations

<sup>5</sup>In NDE applications, estimation of the mean signals and areas of potential defect regions is particularly important for assessing the severity of these regions and their potential to degrade the structural integrity of the testpiece.

<sup>6</sup>See e.g. [8, Ch. 2.3.2] for the definition of a credible set. Here, a 90% credible set for  $\bar{\theta}/\sigma$  and  $A$  is a subset of the space of  $\bar{\theta}/\sigma$  and  $A$  containing 90% of the probability mass from their posterior pdf.

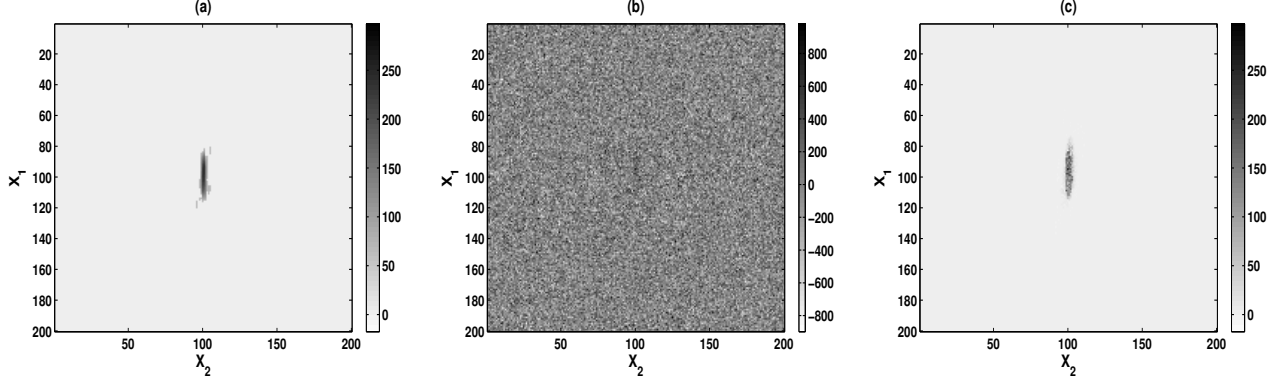


Fig. 5. (a) Signals  $\theta_i$ , (b) simulated noisy observations  $y_i$ , and (c) MMSE estimates  $\hat{\theta}_i$ , for  $i = 1, 2, \dots, N_{\text{tot}}$ .

in Fig. 5 (b), We applied our methods in Sections III-A–III-C to this data set [using (4.1) with  $t_0 = 8,000$  and  $T = 2,000$ ] and obtained the MMSE estimates  $\hat{\theta}_i$  shown in Fig. 5 (c). The proposed method successfully estimates the defect signal from the noisy measurements.

## V. CONCLUDING REMARKS

We developed a hierarchical Bayesian framework for detecting and estimating NDE defect signals from noisy measurements, derived MCMC methods for estimating the defect signal, location, and shape parameters, and successfully applied them to experimental ultrasonic *C*-scan data. Our algorithms are automatic and remarkably easy to implement, requiring only the ability to sample from univariate Gaussian, uniform, and exponential distributions.

Further research will include generalizing the proposed approach to correlated signal and noise models.

### APPENDIX A. IMPLEMENTATION OF THE GIBBS SAMPLING STEPS IN SECTION III-A

#### A. Step 1) of the Gibbs Sampler: Rejection Sampler

We first derive the full conditional posterior pdf of  $\tau$  under the measurement model and prior specifications in Sections II-D and II-E. Note that

$$p(\tau | \mu, \mathbf{z}, \mathbf{y}) \propto (\sigma^2 + \tau^2)^{-N(\mathbf{z})/2} \cdot \exp \left[ -\frac{\sum_{i, \mathbf{s}_i \in \mathcal{R}(\mathbf{z})} (y_i - \mu)^2}{2(\sigma^2 + \tau^2)} \right] \cdot i_{(0, \tau_{\text{MAX}})}(\tau) \triangleq q(\tau | \mu, \mathbf{z}, \mathbf{y}) \quad (\text{A.1})$$

where  $N(\mathbf{z})$  was defined in (3.2) and

$$i_A(x) = \begin{cases} 1, & x \in A, \\ 0, & \text{otherwise} \end{cases} \quad (\text{A.2})$$

denotes the indicator function. We utilize *rejection sampling* to simulate  $\tau$  from  $p(\tau | \mu, \mathbf{z}, \mathbf{y})$ :

- (i) Draw  $\tau$  from  $\pi_\tau(\tau) = \text{uniform}(0, \tau_{\text{MAX}})$ , see (2.10b);
- (ii) Draw  $u$  from  $\text{uniform}(0, 1)$ ;
- (iii) Repeat Steps (i) and (ii) until

$$u \leq \frac{q(\tau | \mu, \mathbf{z}, \mathbf{y})}{\tilde{m}(\mu, \mathbf{z})} \quad (\text{A.3a})$$

where  $\tilde{m}(\mu, \mathbf{z})$  is a bounding constant chosen to guarantee that the right-hand side of the above expression is always between zero and one;

- (iv) Return the  $\tau$  obtained upon exiting the above loop.

Here, we select

$$\tilde{m}(\mu, \mathbf{z}) = \max_{\tau} q(\tau | \mu, \mathbf{z}, \mathbf{y}) = q(\sqrt{\hat{\tau}^2(\mu, \mathbf{z})} | \mu, \mathbf{z}, \mathbf{y})$$

where

$$\hat{\tau}^2(\mu, \mathbf{z}) = \min \left\{ \max \left[ 0, \frac{\sum_{i, \mathbf{s}_i \in \mathcal{R}(\mathbf{z})}^{N(\mathbf{z})} (y_i - \mu)^2}{N(\mathbf{z})} - \sigma^2 \right], \tau_{\text{MAX}}^2 \right\}. \quad (\text{A.3b})$$

To draw  $\tau^{(t)}$  from the conditional pdf (3.4a), we apply the rejection sampling scheme (i)–(iv) with  $\mu$  and  $\mathbf{z}$  replaced by  $\mu^{(t-1)}$  and  $\mathbf{z}^{(t-1)}$ .

### B. Step 2) of the Gibbs Sampler

We derive the full conditional posterior pdf of  $\mu$  under the measurement model and prior specifications in Sections II-D and II-E:

$$p(\mu | \tau, \mathbf{z}, \mathbf{y}) \propto \pi_{\mu}(\mu) \cdot \prod_{i, \mathbf{s}_i \in \mathcal{R}(\mathbf{z})} \mathcal{N}(y_i; \mu, \sigma^2 + \tau^2) \propto \mathcal{N}\left(\mu; \bar{y}(\mathbf{z}), \frac{\sigma^2 + \tau^2}{N(\mathbf{z})}\right) \cdot i_{(0, \mu_{\text{MAX}})}(\mu) \quad (\text{A.4})$$

which is a *truncated Gaussian pdf*. We sample from this pdf using an algorithm similar to that described in [11]. Here,  $\bar{y}(\mathbf{z}) = [1/N(\mathbf{z})] \cdot \sum_{i, \mathbf{s}_i \in \mathcal{R}(\mathbf{z})} y_i$  is the sample mean of the measurements collected over  $\mathcal{R}(\mathbf{z})$ . To draw  $\mu^{(t)}$  from (3.4b), we sample from the truncated Gaussian pdf in (A.4) with  $\tau$  and  $\mathbf{z}$  replaced by  $\tau^{(t)}$  and  $\mathbf{z}^{(t-1)}$ .

### C. Step 3) of the Gibbs Sampler: Shrinkage Slice Sampler

Finally, we discuss sampling from the full conditional posterior pdf of  $\mathbf{z}$  under the measurement and prior models in Sections II-D and II-E:

$$p(\mathbf{z} | \mathbf{w}^{(t)}, \mathbf{y}) \propto \pi_{\mathbf{z}}(\mathbf{z}) \cdot l(\mathbf{y} | \mathbf{z}, \mathbf{w}^{(t)}) \quad (\text{A.5})$$

where  $l(\mathbf{y} | \mathbf{z}, \mathbf{w})$  was defined in (3.1b). Using the approach in [12], we now construct a *shrinkage slice sampling* algorithm to simulate from the above distribution. We first define the initial (largest) hyperrectangle with limits

$$\begin{aligned} x_{0,1,L} &= x_{0,1,\text{MIN}}, & x_{0,1,U} &= x_{0,1,\text{MAX}} \\ x_{0,2,L} &= x_{0,2,\text{MIN}}, & x_{0,2,U} &= x_{0,2,\text{MAX}} \\ d_L &= d_{\text{MIN}}, & d_U &= d_{\text{MAX}} \\ A_L &= A_{\text{MIN}}, & A_U &= A_{\text{MAX}} \\ \varphi_L &= \varphi_{\text{MIN}}, & \varphi_U &= \varphi_{\text{MAX}}. \end{aligned} \quad (\text{A.6})$$

which coincides with the parameter space of  $\phi$ , see Section II-E. We generate  $\mathbf{z}^{(t)}$  from (3.4c) as follows:

- 1) Draw an auxiliary random variable  $u^{(t)}$  from  $\text{uniform}(0, l(\mathbf{y} | \mathbf{z}^{(t-1)}, \mathbf{w}^{(t)}))$  pdf;
- 2) Draw  $x_{0,1}$  from  $\text{uniform}(x_{0,1,L}, x_{0,1,U})$  pdf,  $x_{0,2}$  from  $\text{uniform}(x_{0,2,L}, x_{0,2,U})$ ,  $d$  from  $\text{uniform}(d_L, d_U)$ ,  $A$  from  $\text{uniform}(A_L, A_U)$ , and  $\varphi$  from  $\text{uniform}(\varphi_L, \varphi_U)$ , yielding  $\mathbf{z} = [x_{0,1}, x_{0,2}, d, A, \varphi]^T$ .
- 3) Check if  $\mathbf{z}$  is *within the slice*, i.e.  $l(\mathbf{y} | \mathbf{z}, \mathbf{w}^{(t)}) \geq u^{(t)}$ . (A.7)

If (A.7) holds, return  $\mathbf{z}^{(t)} = \mathbf{z}$  and exit the loop. If (A.7) does not hold, then *shrink the hyperrectangle*:

- If  $x_{0,1} < x_{0,1}^{(t-1)}$ , set  $x_{0,1,L} = x_{0,1}$ ; else if  $x_{0,1} > x_{0,1}^{(t-1)}$ , set  $x_{0,1,U} = x_{0,1}$ .
- If  $x_{0,2} < x_{0,2}^{(t-1)}$ , set  $x_{0,2,L} = x_{0,2}$ ; else if  $x_{0,2} > x_{0,2}^{(t-1)}$ , set  $x_{0,2,U} = x_{0,2}$ .
- If  $d < d^{(t-1)}$ , set  $d_L = d$ ; else if  $d > d^{(t-1)}$ , set  $d_U = d$ .
- If  $A < A^{(t-1)}$ , set  $A_L = A$ ; else if  $A > A^{(t-1)}$ , set  $A_U = A$ .
- If  $\varphi < \varphi^{(t-1)}$ , set  $\varphi_L = \varphi$ ; else if  $\varphi > \varphi^{(t-1)}$ , set  $\varphi_U = \varphi$ .
- Go back to 2).

Here, the hyperrectangles *shrink toward*  $\phi^{(t-1)} = [x_{0,1}^{(t-1)}, x_{0,2}^{(t-1)}, d^{(t-1)}, A^{(t-1)}, \varphi^{(t-1)}]^T$ , which is clearly in the slice, see Step 1).

Since the evaluation of  $l(\mathbf{y} | \mathbf{z}, \mathbf{w})$  may cause a floating-point underflow, it is often safer to compute  $\ln l(\mathbf{y} | \mathbf{z}, \mathbf{w})$  and modify the above algorithm accordingly, see [12, Sect. 4].

#### ACKNOWLEDGMENT

We are grateful to the anonymous reviewers and to Prof. R.B. Thompson from CNDE, Iowa State University, for their insightful comments and for bringing references [1] and [6] to our attention.

#### REFERENCES

- [1] P.J. Howard, D.C. Copley, and R.S. Gilmore, "The application of a dynamic threshold to C-scan images with variable noise," in *Rev. Progress Quantitative Nondestructive Evaluation*, D.O. Thompson and D.E. Chimenti (Eds.), Melville NY: Amer. Inst. Phys., vol. 17, 1998, pp. 2013–2019.
- [2] A. Tsai, A. Yezzi, Jr., and A.S. Willsky, "Curve evolution implementation of the Mumford-Shah functional for image segmentation, denoising, interpolation, and magnification," *IEEE Trans. Image Processing*, vol. 10, pp. 1169–1186, Aug. 2001.
- [3] D.L. Pham, C.Y. Xu, and J.L. Prince, "Current methods in medical image segmentation," *Annu. Rev. Biomed. Eng.*, vol. 2, pp. 315–337, 2000.
- [4] W.E. Polakowski *et al.*, "Computer-aided breast cancer detection and diagnosis of masses using difference of Gaussians and derivative-based feature saliency," *IEEE Trans. Med. Imaging*, vol. 16, pp. 811–819, Sept. 1997.
- [5] A. Dogandžić and B. Zhang, "Bayesian defect signal analysis," to appear in *Proc. 32nd Annu. Review Progress Quantitative Nondestructive Evaluation*, Brunswick, ME, Aug. 2005.
- [6] Aerospace Industries Association Rotor Integrity Sub-Committee, "The development of anomaly distributions for aircraft engine titanium disk alloys," in *Proc. 38th AIAA/ASME/ASCE/AHS/ASC Structures, Structural Dynamics, and Materials Conf.*, Kissimmee, FL, Apr. 1997, pp. 2543–2553. Available online: [http://www.darwin.swri.org/html\\_files/pdf\\_docs/pubs/aia1997.pdf](http://www.darwin.swri.org/html_files/pdf_docs/pubs/aia1997.pdf).
- [7] A. Gelman, J.B. Carlin, H.S. Stern, and D.B. Rubin, *Bayesian Data Analysis*, 2nd. ed., New York: Chapman & Hall, 2004.
- [8] B.P. Carlin and T.A. Louis, *Bayes and Empirical Bayes Methods for Data Analysis*, 2nd. ed., New York: Chapman & Hall, 2000.
- [9] C.P. Robert and G. Casella, *Monte Carlo Statistical Methods*, 2nd. ed., New York: Springer-Verlag, 2004.
- [10] J. von Neumann, "Various techniques used in connection with random digits," *National Bureau of Standards Applied Mathematics Series*, vol. 12, pp. 36–38, 1951.
- [11] J. Geweke, "Efficient simulation from the multivariate normal and Student-t distributions subject to linear constraints," in *Computing Science and Statistics: Proc. 23rd Symposium on the Interface*, Seattle, WA, Apr. 1991, pp. 571–578.
- [12] R.M. Neal, "Slice sampling," *Ann. Statist.*, vol. 31, pp. 705–741, Jun. 2003.
- [13] C. Andrieu, A. Doucet, and C.P. Robert, "Computational advances for and from Bayesian analysis," *Statistical Science*, vol. 19, no. 1, pp. 118–127, Feb. 2004.
- [14] D.J. Spiegelhalter, N.G. Best, B.R. Carlin, and A. van der Linde, "Bayesian measures of model complexity and fit," *J. R. Stat. Soc., Ser. B*, vol. 64, pp. 583–639, 2002.

## LIST OF FIGURES

1	Ultrasonic $C$ -scan data with 17 defects. . . . .	7
2	MMSE estimates $\hat{\theta}_i$ of the random signals $\theta_i$ for the chains having the smallest model-parameter deviances. . . . .	8
3	Estimated model-parameter deviances for the potential defects in Region 1,2, and 3, respectively. . . . .	8
4	Approximate 90% credible sets for the normalized mean signals $\bar{\theta}/\sigma$ and areas $A$ of all potential defects in the three regions and a possible classification boundary for separating defects from non-defects. . . . .	9
5	(a) Signals $\theta_i$ , (b) simulated noisy observations $y_i$ , and (c) MMSE estimates $\hat{\theta}_i$ , for $i = 1, 2, \dots, \mathbb{N}_{\text{tot}}$ . . . . .	10

